

Nonlinear theory of transverse beam echoes

Tanaji Sen *

Accelerator Physics Center, FNAL, Batavia, IL 60510

Yuan Shen Li †

Carleton College, Northfield, MN 55057

Abstract

Transverse beam echoes can be excited with a single dipole kick followed by a single quadrupole kick. They have been used to measure diffusion in hadron beams and have other diagnostic capabilities. Here we develop theories of the transverse echo nonlinear in both the dipole and quadrupole kick strengths. The theories predict the maximum echo amplitudes and the optimum strength parameters. We find that the echo amplitude increases with smaller beam emittance and the asymptotic echo amplitude can exceed half the initial dipole kick amplitude. We show that multiple echoes can be observed provided the dipole kick is large enough. The spectrum of the echo pulse can be used to determine the nonlinear detuning parameter with small amplitude dipole kicks. Simulations are performed to check the theoretical predictions. In the useful ranges of dipole and quadrupole strengths, they are shown to be in reasonable agreement.

1 Introduction

Echoes are ubiquitous phenomena in physics. Spin echoes were discovered by Hahn [1] and since then, spin echoes have evolved into use as sophisticated diagnostic tools in magnetic resonance imaging [2]. Photon echoes were observed from a ruby crystal after excitation by a sequence of two laser pulses, each about $0.1\mu\text{s}$ long [3]. Later, plasma wave echoes were predicted and then observed in a plasma excited by two rf pulses [4, 5]. A system of ultra-cold atoms confined within an optical trap exhibited echoes when excited by a sequence of microwave pulses [6]. About a decade ago, fluid echoes were observed in a magnetized electron plasma [7]. More recently, so called fractional echoes were observed in a CO_2 gas excited by two femtosecond laser pulses [8]. Echoes were first introduced into accelerator physics more than two decades ago [9, 10]. This was followed by the observation of longitudinal echoes in unbunched beams first at the Fermilab Antiproton

*tsen@fnal.gov

†Present address: Dept. of Physics, University of Chicago, Chicago, IL 60637

Accumulator [11] and later at the SPS [12]. Transverse echoes were seen at the SPS [13], but more detailed studies with transverse bunched beam echoes were performed at RHIC [14]. A detailed analysis of these experiments to extract diffusion coefficients was recently reported in [15].

In all echo phenomena, the system (atoms, plasma, particle beam etc.) is first acted on by a pulsed excitation (e.g. a dipole kick on a beam) that excites a coherent response which then decoheres due to phase mixing. However the information in the macroscopic observables (coordinate moments for a particle beam) is not lost, but can be retrieved by the application of a second pulsed excitation (e.g. a quadrupole kick). Some time after the response to the second excitation has disappeared, a coherent response, called the echo, reappears. The strength of the echo signal in a beam depends on the beam parameters and on the strengths of the kicks from the magnets. The echo response is exquisitely sensitive to the presence of beam diffusion. This sensitivity simultaneously presents both opportunities and challenges. The short time scale over which beam echoes can be measured (typically within a few thousand turns in an accelerator ring) implies that diffusion can be measured very quickly compared to the conventional method of using movable collimators e.g. [16], which can take hours. However, the echo signal can also be destroyed by strong diffusion. It is therefore necessary to understand how to maximize the echo response by appropriate choices of beam parameters and excitation strengths.

In this paper we develop a theory of echoes in one degree of freedom with nonlinear dependence on dipole and quadrupole strengths, with the goal of maximizing the echo signal. A nonlinear theory had been developed earlier in [10]. Here we follow a different approach, the method as described in [17] where it was restricted to a linear theory. Our results are more general than those in [10], but reduce to them in limiting cases. In Section II, we develop a theory (labeled QT) that is linear in the dipole kick, but nonlinear in the quadrupole kick strength. This is followed in Section III with a simplified echo theory (labeled DQT) that is nonlinear in both dipole and quadrupole kick strengths; a more complete theory is described in Appendix A. Section IV discusses simulations performed to check the theoretical results. Section V shows how the spectrum of the echo pulse can be used to extract the detuning parameter and we end in Section VI with our conclusions.

2 Nonlinear theory of quadrupole kicks

The simplest way to generate a transverse beam echo is to apply a short pulse dipole kick, usually done with an injection kicker, to a beam in an accelerator ring with nonlinear elements so that the betatron tune is amplitude dependent. The centroid motion decoheres due to the tune spread [18] and at some time τ after the dipole kick, the beam is excited with a short pulse quadrupole kick. For simplicity we will consider a single turn quadrupole kick, although this is strictly not necessary and this kick could last a few turns. Following the quadrupole kick, the decoherence starts to partially reverse and at time 2τ after the dipole kick, the first echo appears. Depending on beam parameters and kick strengths, multiple echoes can appear at times 4τ , 6τ etc.

The echo amplitude depends on several parameters, especially the dipole and quadrupole kick strengths. Our approach will be to develop an Eulerian theory by following the flow of the density distribution, similar to the development in [17] where both kicks were treated in linearized approximations. In this section, we develop a theory (labeled QT) that is linear in the dipole strength but nonlinear in the quadrupole strength. We will compare our results with those from an alternative method of following the particle's phase space motion that had been developed earlier [10]. As mentioned in the Introduction, the treatment here is for motion in one transverse degree of freedom, so the effects of transverse coupling as well as coupling to the effects of synchrotron oscillations and energy spread are ignored here. We also do not consider here how diffusion reduces the echo amplitudes or the impact of collective effects at high intensity. These are important effects which will be considered elsewhere.

We start with the usual definitions of the phase space variables in position and momentum (x, p) and the corresponding action and angle variables (J, ϕ)

$$x = \sqrt{2\beta J} \cos \phi, \quad p = \beta x' + \alpha x = -\sqrt{2\beta J} \sin \phi \quad (2.1)$$

$$J = \frac{1}{2\beta} [x^2 + p^2], \quad \phi = \text{Arctan}\left(\frac{-p}{x}\right) \quad (2.2)$$

We will assume that the nonlinear motion of the particles can be modeled by an action dependent betatron frequency and for simplicity we assume the form

$$\omega(J) = \omega_\beta + \omega' J \quad (2.3)$$

where ω_β is the bare angular betatron frequency, and ω' is the frequency slope which is determined by the lattice nonlinearities. This model therefore assumes that the effects of nearby resonances are negligible. We assume that the initial particle distribution is a Gaussian in (x, p) or equivalently an exponential in the action

$$\psi_0(J) = \frac{1}{2\pi\epsilon_0} \exp\left[-\frac{J}{\epsilon_0}\right] \quad (2.4)$$

with initial emittance ϵ_0 . At time $t = 0$, an impulsive single turn dipole kick $\Delta p = \beta_K \Delta x' = \beta_K \theta$ changes the distribution function (DF) to $\psi_1(J, \phi) = \psi_0(x, p - \beta_K \theta)$ where β_K is the beta function at the dipole and θ is the kick angle. To first order in the dipole kick, we have

$$\psi_1(J, \phi) = \psi_0(J) + \beta_K \theta \psi_0'(J) \sqrt{\frac{2J}{\beta}} \sin \phi \quad (2.5)$$

Following the dipole kick, the action remains constant while the angle ϕ evolves by a free betatron rotation. Hence, at time t after the dipole kick, the DF is

$$\psi_2(J, \phi, t) = \psi_0(J) + \beta_K \theta \psi_0'(J) \sqrt{\frac{2J}{\beta}} \sin(\phi - \omega(J)t) \quad (2.6)$$

Just before the quadrupole kick at time τ , the DF is $\psi_3(J, \phi, \tau) = \psi_2(J, \phi, t = \tau)$. The first term $\psi_0(J)$ in the perturbed DF does not contribute to the dipole moment, and it will

be dropped in the rest of this section. The quadrupole kick $\Delta p = -qx$ changes the distribution to $\psi_4(x, p, \tau) = \psi_3(x, p + qx, \tau)$. Here $q = \beta_Q/f$ is the dimensionless quadrupole strength parameter, with β_Q the beta function at the quadrupole and f the focal length of this quadrupole. In practical applications $q \ll 1$ and we will assume this to be true in the development here.

Due to this quadrupole kick, the action and angle arguments of the density distribution change to

$$J \rightarrow \frac{1}{2\beta} [x^2 + (p + qx)^2] \equiv J[1 + A(q, \phi)], \quad A(q, \phi) = (-q \sin 2\phi + q^2 \cos^2 \phi) \quad (2.7)$$

$$\phi \rightarrow \text{Arctan}\left(-\frac{p + qx}{x}\right) = \text{Arctan}(\tan \phi - q) \quad (2.8)$$

To proceed, we have to approximate the form of the transformed angle variable. A Taylor expansion shows that

$$\text{Arctan}(\tan \phi - q) = \phi - q \cos^2 \phi - \frac{1}{4} q^2 (\sin 2\phi + \frac{1}{2} \sin 4\phi) + O(q^3) \quad (2.9)$$

For reasons of simplicity, we will keep terms to $O(q)$ in this expansion. For self-consistency, we consider $A(q, \phi)$ to the same order and approximate $A(q, \phi) \approx -q \sin 2\phi$. While the Jacobian of the exact transformation has a determinant of one, the approximate transform has the determinant $= 1 + O(q^2)$.

The DF right after the quadrupole kick with the approximation above is given by,

$$\psi_4(J, \phi, \tau) = \beta_K \theta \psi'_0(J[1 - q \sin 2\phi]) \sqrt{\frac{2J(1 - q \sin 2\phi)}{\beta}} \sin[\phi_{-\tau} - q \cos^2 \phi] \quad (2.10)$$

$$\phi_{-\tau} = \phi - \omega(J[1 - q \sin 2\phi])\tau \quad (2.11)$$

Following the quadrupole kick, the DF at time t (from the instant of the dipole kick) is

$$\psi_5(J, \phi, t) = \psi_4(J, \phi_{-\Delta\phi}), \quad \phi_{-\Delta\phi} \equiv \phi - \Delta\phi, \quad \Delta\phi = \omega(J)(t - \tau) \quad (2.12)$$

We note that as defined here, $\Delta\phi$ depends on the action J but is independent of the angle ϕ . Under the change $\phi \rightarrow \phi_{-\Delta\phi}$, the angle variable $\phi_{-\tau}$ transforms as $\phi_{-\tau} \rightarrow \phi_{-\Delta\phi} - \tau\omega + q\tau\omega'J \sin 2\phi_{-\Delta\phi}$. The dipole moment at time t is

$$\begin{aligned} \langle x \rangle(t) &= \sqrt{2\beta} \int dJ \int d\phi \sqrt{J} \cos \phi \psi_5(J, \phi, t) \\ &= 2\beta_K \theta \int dJ \int d\phi \sqrt{J} \cos \phi \psi'_0(J[1 - q \sin 2\phi_{-\Delta\phi}]) \sqrt{J[1 - q \sin 2\phi_{-\Delta\phi}]} \\ &\quad \times \sin\left(\phi_{-\Delta\phi} - \frac{1}{2}q(1 + \cos 2\phi_{-\Delta\phi}) - \tau\omega + q\tau\omega'J \sin 2\phi_{-\Delta\phi}\right) \end{aligned} \quad (2.13)$$

We proceed by simplifying the trigonometric terms in the argument of the first sine function in the last line above

$$\begin{aligned} -\frac{1}{2} \cos 2\phi_{-\Delta\phi} + \tau\omega'J \sin 2\phi_{-\Delta\phi} &= \sqrt{(\tau\omega'J)^2 + \frac{1}{4}} \sin[2\phi_{-\Delta\phi} - \text{Arctan}\left(\frac{1}{2\tau\omega'J}\right)] \\ &\approx \tau\omega'J \sin 2\phi_{-\Delta\phi} \end{aligned} \quad (2.14)$$

where the last approximation follows by noting that the decoherence time $\tau_D \simeq \omega' \varepsilon_0$ is much shorter than the delay time τ , hence $\tau \omega' \varepsilon_0 \simeq \tau / \tau_D \gg 1$. Next, we expand the square root to first order in q as $\sqrt{[1 - q \sin 2\phi - \Delta\phi]} \approx [1 - \frac{1}{2}q \sin 2\phi - \Delta\phi]$.

Hence we can write

$$\langle x(t) \rangle = -\frac{\beta_K \theta}{2\pi \varepsilon_0^2} \int J \exp\left[-\frac{J}{\varepsilon_0}\right] \{S_1 - S_2 + S_3 - S_4\} dJ \equiv T_1 - T_2 + T_3 - T_4 \quad (2.15)$$

The terms S_i are obtained after integrating over ϕ and are given by

$$S_1 = -2\pi \operatorname{Im} \left\{ \exp\left[i\left(\Delta\phi - \tau\omega - \frac{1}{2}q\right)\right] J_1(q\tau\omega'J) \right\} \quad (2.16)$$

$$S_2 = 2\pi \operatorname{Im} \left\{ \exp\left[i\left(\Delta\phi + \tau\omega + \frac{1}{2}q\right)\right] J_0(q\tau\omega'J) \right\} \quad (2.17)$$

$$S_3 = -\frac{\pi}{2} q \operatorname{Re} \left\{ \exp\left[i\left(-\Delta\phi + \tau\omega + \frac{1}{2}q\right)\right] J_0(q\tau\omega'J) - \exp\left[i\left(\Delta\phi - \tau\omega - \frac{1}{2}q\right)\right] J_2(q\tau\omega'J) \right\} \quad (2.18)$$

$$S_4 = \frac{\pi}{2} \operatorname{Re} \left\{ \exp\left[-i\left(\Delta\phi + \tau\omega + \frac{1}{2}q\right)\right] J_{-1}(q\tau\omega'J) + \exp\left[i\left(\Delta\phi + \tau\omega\right)\right] J_1(q\tau\omega'J) \right\} \quad (2.19)$$

where the integrals over ϕ were done by first expanding into Bessel functions and using

$$\begin{aligned} \int d\phi \exp[im\phi] \exp[ia \sin(2\phi - 2\Delta\phi)] &= \int d\phi \exp[im\phi] \sum_k J_k(a) \exp[ik(2\phi - 2\Delta\phi)] \\ &= 2\pi J_{-m/2}(a) \exp[im\Delta\phi] \end{aligned} \quad (2.20)$$

We clarify that J denotes the action while J_n with a subscript n will denote the Bessel function.

To integrate over the action J , we introduce the dimensionless integration variable $z = J/\varepsilon_0$ and define the following dimensionless parameters that are independent of the action,

$$\Phi = \omega_\beta(t - 2\tau), \quad \xi(t) = (t - 2\tau)\omega' \varepsilon_0, \quad Q = q\tau\omega' \varepsilon_0 \quad (2.21)$$

$$a_1 = 1 - i\xi, \quad a_2 = 1 - i\omega' t \varepsilon_0 \quad (2.22)$$

It follows that the terms T_i , obtained by integrating over J in Eq. (2.15), are

$$T_1 = \beta_K \theta \operatorname{Im} \left\{ \exp\left[i\left(\Phi - \frac{1}{2}q\right)\right] H_{1,1}(a_1, Q) \right\} \quad (2.23)$$

$$T_2 = -\beta_K \theta \operatorname{Im} \left\{ \exp\left[i\left(\omega_\beta t + \frac{1}{2}q\right)\right] H_{1,0}(a_2, Q) \right\} \quad (2.24)$$

$$T_3 = -\frac{1}{4} \beta_K \theta q \operatorname{Re} \left\{ \exp\left[-i\left(\Phi - \frac{1}{2}q\right)\right] H_{1,0}(a_1^*, Q) - \exp\left[i\left(\Phi - \frac{1}{2}q\right)\right] H_{1,2}(a_1, Q) \right\} \quad (2.25)$$

$$T_4 = \frac{1}{4} \beta_K \theta \varepsilon_0^2 q \operatorname{Re} \left\{ \exp\left[-i\left(\omega_\beta t + \frac{1}{2}q\right)\right] H_{1,1}(a_2^*, Q) + \exp\left[i\left(\omega_\beta t + \frac{1}{2}q\right)\right] H_{1,1}(a_2, Q) \right\} \quad (2.26)$$

where a_1^* is the complex conjugate of a_1 and the functions $H_{m,n}(a, Q)$ are defined as

$$H_{m,n}(a, Q) = \int_0^\infty dz z^m \exp[-az] J_n(Qz) \quad (2.27)$$

Consider only the terms with phases that depend on Φ rather than on $\omega_\beta t$. These phase terms will vanish around the time of the echo at $t = 2\tau$ and the terms T_1, T_3 will be the dominant terms to determine the echo amplitude.

$$T_1 = \beta_K \theta \operatorname{Im} \left\{ \exp[i(\Phi - \frac{1}{2}q)] \frac{Q}{(a_1^2 + Q^2)^{3/2}} \right\} \quad (2.28)$$

$$T_3 = -\frac{1}{4} \beta_K \theta q \operatorname{Re} \left\{ \exp[-i(\Phi - \frac{1}{2}q)] \frac{a_1^*}{((a_1^*)^2 + Q^2)^{3/2}} \right. \\ \left. - \exp[i(\Phi - \frac{1}{2}q)] \frac{2(a_1^2 + Q^2)^{3/2} - a_1(2a_1^2 + 3Q^2)}{Q^2(a_1^2 + Q^2)^{3/2}} \right\} \quad (2.29)$$

In order to simplify the evaluation of these terms, we introduce the amplitude functions $A_0(t; \tau, q), A_1(t; \tau, q)$, the phase functions $\Theta(t; \tau, q), \Theta_1(t; \tau, q)$ and two other terms a_{3C}, a_{3S} as follows

$$(a_1^2 + Q^2)^{3/2} \equiv A \exp[-i3\Theta], \quad a_1 \equiv A_1(t; \tau, q) \exp[i\Theta_1] \quad (2.30)$$

$$A_0(t; \tau, q) = [(1 - \xi^2 + Q^2)^2 + 4\xi^2]^{3/4}, \quad \Theta = \operatorname{Arctan}\left[\frac{\xi}{1 - \xi^2 + Q^2}\right] \quad (2.31)$$

$$A_1 = [1 + \xi^2]^{1/2}, \quad \Theta_1 = \operatorname{Arctan}[\xi] \quad (2.32)$$

$$a_{3C} = -\frac{1}{2}q \left(A_1 \cos(3\Theta + \Theta_1) - \frac{A_0}{Q^2} + \frac{A_0^{2/3} A_1}{Q^2} \cos(\Theta + \Theta_1) \right) \quad (2.33)$$

$$a_{3S} = -\frac{1}{2}q \left(A_1 \sin(3\Theta + \Theta_1) + \frac{A_0^{2/3} A_1}{Q^2} \sin(\Theta + \Theta_1) \right) \quad (2.34)$$

In terms of these amplitudes and phases, the functions T_1, T_3 simplify to

$$T_1 = \frac{\beta_K \theta Q}{A_0} \sin[\Phi - \frac{1}{2}q + 3\Theta], \quad T_3 = -\frac{\beta_K \theta}{A_0} \left[a_{3C} \cos(\Phi - \frac{1}{2}q) - a_{3S} \sin(\Phi - \frac{1}{2}q) \right] \quad (2.35)$$

Keeping these two dominant terms at large times, we can write the time dependent echo in terms of an amplitude and phase as

$$\langle x(t) \rangle = T_1 + T_3 = \beta_K \theta A_{1,3} \sin(\Phi(t) + \Theta_{1,3}(t) - \frac{1}{2}q) \quad (2.36)$$

$$A_{1,3} = \frac{1}{A_0} [(Q \cos 3\Theta + a_{3S})^2 + (Q \sin 3\Theta - a_{3C})^2]^{1/2} \quad (2.37)$$

$$\Theta_{1,3} \equiv \operatorname{Arctan} \left[\frac{Q \sin 3\Theta - a_{3C}}{Q \cos 3\Theta + a_{3S}} \right] \quad (2.38)$$

We consider various limiting forms of this general form of the echo (in the linearized dipole kick approximation of this section) below.

Of the two terms, T_1 has the dominant contribution to the echo amplitude. Keeping only this term, the time dependent amplitude is

$$\langle x(t) \rangle \approx \beta_K \theta \frac{Q}{[(1 - \xi^2(t) + Q^2)^2 + 4\xi^2(t)]^{3/4}} \sin[\Phi(t) + 3\Theta(t) - \frac{1}{2}q] \quad (2.39)$$

The echo amplitude at $t = 2\tau$ is approximated by

$$\langle x(t = 2\tau) \rangle^{amp} \approx \beta_K \theta \frac{Q}{(1 + Q^2)^{3/2}} \quad (2.40)$$

This expression has the same form as Eq. (4.10) in [10] evaluated at the time of the first echo. We expect however that the general form in Eq. (2.36) will be more accurate for larger values of q . Finally we recover the completely linear theory by dropping the Q^2 term. In this case $\Theta(t) \approx \text{Arctan}[\xi(t)]$ and we have

$$\langle x(t) \rangle_{linear} = \beta_K \theta \frac{Q}{[(1 + \xi^2(t))]^{3/2}} \sin(\Phi(t) + 3\text{Arctan}[\xi(t)] - \frac{1}{2}q) \quad (2.41)$$

Eq. (2.41) is the same as that obtained in [17], with the addition of the small correction to the phase. The range of values in the quadrupole strength q over which the linear theory is valid decreases as either the emittance or the dipole kick increases.

In order to obtain the optimum quadrupole strength that maximizes the echo amplitude, we define a dimensionless parameter $\eta = \omega' \epsilon_0 \tau = \tau / \tau_D$ in terms of which $Q = q\eta$. Let $\sigma_0 = \sqrt{\beta \epsilon_0}$ denote the rms beam size at a location with beta function β . Then η is the additional change in phase due to the nonlinearity of particles at the rms beam size accumulated in the time between the two kicks. The optimum quadrupole kick q_{opt} at which the echo amplitude reaches a maximum when $\eta \gg 1$ is given by

$$\lim_{\eta \gg 1} q_{opt} = \frac{1}{\sqrt{2}\eta} = \frac{1}{\sqrt{2}} \frac{1}{\omega' \epsilon_0 \tau} \quad (2.42)$$

Proceeding with the above form for q_{opt} , and substituting back into the simpler Eq. (2.40), the echo amplitude relative to the dipole kick at the optimum quadrupole strength

$$\lim_{\eta \gg 1} A_{max} \equiv \lim_{\eta \gg 1} \frac{\langle x(2\tau) \rangle^{max,amp}}{\beta_K \theta} = \frac{2}{3\sqrt{3}} = 0.38 \quad (2.43)$$

The results for q_{opt} and A_{max} in this approximation of keeping only T_1 were first obtained in [10]. In this form, the maximum relative amplitude A_{max} is a constant, independent of the initial emittance and dipole kick. We expect this to be true when the initial emittance is sufficiently large. We note that the value of A_{max} observed with gold ions with their nominal emittances during the RHIC experiments [14] was 0.35, close to this predicted value. Numerical evaluation of the complete amplitude function $A_{1,3}$ defined in Eq. (2.37) leads to a correction of about 10% from that in Eq. (2.43). The simulations to be discussed in Section 4 will show that A_{max} exceeds the above prediction for small emittances.

The above discussion has assumed that the rms angular betatron frequency spread is given by $\sigma_\omega = \omega' \epsilon_0$. However, the beam decoheres following the dipole kick and the

emittance grows from ε_0 to $\varepsilon_f = \varepsilon_0[1 + \frac{1}{2}(\beta_K\theta/\sigma_0)^2]$ at times $t \gg \tau_D$ [19, 15]. At these times, we assume that the increased rms frequency spread can be approximated by $\sigma_\omega \approx \omega'\varepsilon_f$. In the next section, we will calculate this rms frequency spread exactly and show that this approximation is valid in the limit of small amplitude dipole kicks $\beta_K\theta \ll \sigma_0$. Incorporating this increased emittance and frequency spread had turned out to be essential in comparing theory with the experimental measurements at RHIC [15]. We can include these effects into the above equations by the approximate modifications

$$\xi(t) \approx (t - 2\tau)\omega'\varepsilon_0[1 + \frac{1}{2}(\frac{\beta_K\theta}{\sigma_0})^2] \quad (2.44)$$

$$Q \approx q\tau\omega'\varepsilon_0[1 + \frac{1}{2}(\frac{\beta_K\theta}{\sigma_0})^2] \quad (2.45)$$

These changes lead to a theory which is nonlinear in the dipole kick but this is an incomplete dependence. A more complete nonlinear theory will be discussed in the next section.

The plots in Figure 1 show the echo amplitude dependence on the quadrupole kick, as predicted by Eq. (2.36) with and without the modifications introduced in Eqs. (2.44) and (2.45). For a very small initial emittance (left plot), the black curve shows that the relative echo amplitude without emittance growth is independent of the dipole kick and increases monotonically with the quadrupole kick; the relative amplitude reaches nearly 0.5 at $q = 1$. The blue and red curves for dipole kicks of 1mm and 3mm respectively include the increased frequency spread which changes the profiles significantly. In both cases, A_{max} is close to 0.38, while q_{opt} shifts to lower values. The right plot in Fig. 1 shows results with a larger initial emittance chosen close to measured values in the RHIC experiments [14]. In this case, even without including the increased emittance from the dipole kick, A_{max} does not exceed 0.38. Including the increased frequency spread shifts q_{opt} to lower values, as expected since $q_{opt} \propto 1/\sigma_\omega$. The two plots combined also show that q_{opt} decreases with increasing emittance.

3 Nonlinear theory of dipole and quadrupole kicks

There are a few drawbacks to the theory developed in the previous section. The first is that it has an incomplete dependence on the dipole kick strength; the emittance growth had to be introduced as a correction. The value of A_{max} is limited to 0.38, in disagreement with simulation results. It also does not predict the existence of multiple echoes at times beyond the first one at 2τ . However the experiments at RHIC (cf. Fig. 5 in [14]) showed echoes at 4τ and 6τ . These multiple echoes are also seen in simulations, see. Fig. 9 in Section 4. Our aim is to develop a theory, labeled DQT, that is nonlinear in both dipole and quadrupole strengths which will remove these drawbacks.

In this section, we will make an approximation for the change in the distribution function that includes the large time dependent change in the angle ϕ but neglects the smaller impulsive changes to the action and angle. This results in expressions which are approximate but contain the essential physics. The more complete theory which results in more complicated expressions is developed in Appendix A.

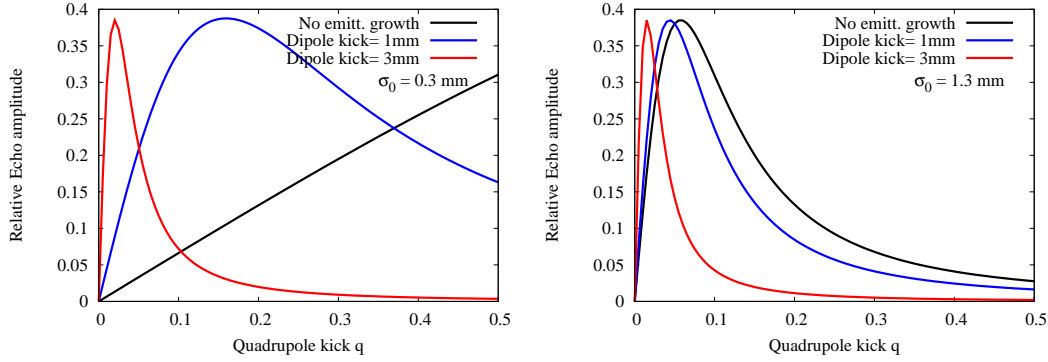


Figure 1: The echo amplitude relative to the dipole kick as a function of quadrupole kick predicted by Eq. (2.36). The two plots are for different initial emittances. In each plot, the black curve shows the prediction without including the emittance growth from a dipole kick, the blue and red curves include emittance growth from dipole kicks of 1mm and 3mm respectively.

Using the notation of Section 2, the complete distribution function (DF) without the first order Taylor expansion at time t after the dipole kick is

$$\psi_2(J, \phi, t) = \psi_0(J + \beta_K \theta \sqrt{2J/\beta} \sin \phi_{-t} + (1/2)\beta_K \theta^2), \quad \phi_{-t} \equiv \phi - \omega(J)t \quad (3.1)$$

This DF can be used to calculate the increased emittance and the tune spread after the dipole kick. The time dependent rms emittance was calculated in [15]. The action dependent frequency spread is $\Delta\omega = \omega'J$ from which the rms frequency spread σ_ω can be found from

$$\sigma_\omega = \sqrt{\langle(\Delta\omega)^2\rangle - (\langle\Delta\omega\rangle)^2}, \quad \langle\Delta\omega\rangle = \omega' \int dJ J \int d\phi \psi_2(J, \phi, t) \quad (3.2)$$

Using the form of ψ_2 in Eq. (3.1), we find that the exact rms frequency spread after the dipole kick is

$$\sigma_\omega = \omega' \varepsilon_0 \sqrt{1 + \frac{\beta_K \theta^2}{\varepsilon_0}} \quad (3.3)$$

In the limit of small amplitude dipole kicks, this reduces to the approximate form assumed in Eq.(2.44) and Eq. (2.45). The increase in the frequency spread leads to a smaller decoherence time after the dipole kick, as will also be seen in the simulations.

We follow the same transformations as in Section 2 to calculate the centroid motion following the quadrupole kick at time $t = \tau$. The dominant contribution to the change in the DF after the quadrupole kick at time $t > \tau$ is the transformation due to the angle evolution $\phi_{-\tau} \rightarrow \phi_{-\Delta\phi} - \tau\omega + Q(J/\varepsilon_0) \sin 2\phi_{-\Delta\phi}$ because these grow with time as $(t - \tau)$ and the delay τ (Q depends on τ). The theory in Appendix A includes the smaller transformations due to the impulsive kicks. Here, in the approximation of keeping only this dominant term, the DF as a function of the scaled action variable $z = J/\varepsilon_0$ at a time after the quadrupole

kick $t > \tau$ is

$$\psi_5(z, \phi, t) = \psi_0(z\varepsilon_0 + \beta_K \theta \sqrt{\frac{2\varepsilon_0 z}{\beta}} \sin(\phi_{-\Delta\phi} - \tau\omega - q \cos^2 \phi_{-\Delta\phi} + Qz \sin 2\phi_{-\Delta\phi}) + \frac{1}{2}\beta_K \theta^2) \quad (3.4)$$

We have for the dipole moment

$$\langle x(t) \rangle = \frac{\sqrt{2\beta\varepsilon_0}}{2\pi} \exp\left[-\frac{\beta_K \theta^2}{2\varepsilon_0}\right] \int dz \sqrt{z} \exp[-z] T_\phi(z) \quad (3.5)$$

$$T_\phi(z) \simeq \text{Re} \left\{ \int d\phi e^{i\phi} \exp\left[-a_\theta \sqrt{2z} \sin(\phi_{-\Delta\phi} - \tau\omega - \frac{1}{2}q + Qz \sin 2\phi_{-\Delta\phi})\right] \right\} \quad (3.6)$$

where we introduced the dimensionless dipole kick parameter in units of the rms beam size

$$a_\theta = \frac{\beta_K \theta}{\sqrt{\beta\varepsilon_0}} \quad (3.7)$$

One way of doing the ϕ integration is to use the generating functions for the modified Bessel function $I_n(z)$ and for the Bessel function $J_n(z)$ [21], i.e.

$$e^{-z \sin \theta} = \sum_{n=-\infty}^{\infty} i^n I_n(z) e^{in\theta}, \quad e^{iz \sin \theta} = \sum_{l=-\infty}^{\infty} J_l(z) e^{il\theta}$$

Then the term $T_\phi(z)$ transforms to

$$\begin{aligned} T_\phi(z) &= \text{Re} \left\{ \sum_{k=-\infty}^{\infty} \sum_{l=-\infty}^{\infty} i^k I_k(a_\theta \sqrt{2z}) J_l(kQz) \exp\left[i\left(-k(\Delta\phi + \tau\omega + \frac{1}{2}q) - 2l\Delta\phi\right)\right] \right. \\ &\quad \left. \times \int d\phi \exp\left[i\left([1+k+2l]\phi\right)\right] \right\} \\ &= 2\pi \text{Re} \left\{ \sum_l i^{-(2l+1)} I_{-(2l+1)}(a_\theta \sqrt{2z}) J_l(-(2l+1)Qz) \right. \\ &\quad \left. \times \exp\left[i\left(\omega(t+2l\tau) + \frac{1}{2}(2l+1)q\right)\right] \right\} \quad (3.8) \end{aligned}$$

Since the sum extends over positive and negative values of l , we can replace $l = -n$ and write

$$\omega(t-2n\tau) \equiv \Phi_n + \xi_n z, \quad \Phi_n = \omega_\beta(t-2n\tau), \quad \xi_n = \omega' \varepsilon_0(t-2n\tau) \quad (3.9)$$

We have therefore for the time dependent echo pulse

$$\begin{aligned} \langle x(t) \rangle &= \sqrt{2\beta\varepsilon_0} e^{-(\beta/2\beta_K)a_\theta^2} \text{Im} \left\{ \sum_{n=-\infty}^{\infty} \exp\left[i\left(\Phi_n - \frac{1}{2}(2n-1)q\right)\right] \right. \\ &\quad \left. \times \int dz \sqrt{z} \exp[-z(1-i\xi_n)] I_{2n-1}(a_\theta \sqrt{2z}) J_n([2n-1]Qz) \right\} \quad (3.10) \end{aligned}$$

where we used $\text{Re}[-if(z)] = \text{Im}[f(z)]$ for a complex function $f(z)$. This echo pulse will be large when the dominant phase factors $\Phi_n = 0 = \xi_n$, i.e at times $t = 2n\tau$. This form therefore predicts echoes at times close to multiples of 2τ . The presence of the small q dependent phase factor i.e. $(2n-1)q/2$ will shift the maximum of the echo away from $2n\tau$, the shift increasing with q and the order n of the echo. The dipole moment of the first echo ($n = 1$), under the approximations made in this section, is

$$\begin{aligned} \langle x(t = 2\tau) \rangle &= \sqrt{2\beta\epsilon_0} e^{-(\beta/2\beta_K)a_\theta^2} \text{Im} \left\{ e^{i(\Phi_1 - q/2)} \right. \\ &\quad \left. \times \int dz \sqrt{z} \exp[-z\{1 - i\xi_1\}] I_1(a_\theta\sqrt{2z}) J_1(Qz) \right\} \end{aligned} \quad (3.11)$$

This form can be compared with the term T_1 in Section 2 in the linear dipole approximation, which was (before the integration over z)

$$\langle x(t = 2\tau) \rangle_{QT} = \beta_K \theta \text{Im} \left\{ e^{i(\Phi_1 - q/2)} \int dz z \exp[-z\{1 - i\xi_1\}] J_1(Qz) \right\} \quad (3.12)$$

If in Eq. (3.11) we replace $I_1(a_\theta\sqrt{2z})$ by its first order approximation $\frac{1}{2}a_\theta\sqrt{2z}$ and $e^{-(\beta/2\beta_K)a_\theta^2}$ by 1, then it reduces to Equation 3.12. In Section 2, we included the emittance growth due to the dipole kick in a post hoc fashion by changing ϵ_0 to ϵ_f in parameters such as ξ , Q etc. In this section, the use of the complete distribution function to all orders in the dipole kick, e.g. ψ_3 in Eq. (3.1), naturally accounts for the emittance growth as is seen by calculating the second moments [15]. Hence we use the original definitions of the parameters ξ , Q in evaluating Eq. (3.11). This equation shows that the maximum relative echo amplitude depends on the relative dipole kick a_θ through $\exp[-(\beta/(2\beta_K))a_\theta^2] I_1(\sqrt{2}a_\theta\sqrt{z})$ and on the quadrupole strength q , the emittance ϵ_0 , the lattice nonlinearity ω' , and the delay τ through $J_1(q\omega'\tau\epsilon_0 z)$.

The amplitude of the echo at 4τ corresponds to the term with $n = 2$ in Eq. (3.10). Hence

$$\begin{aligned} \langle x(t = 4\tau) \rangle &= \sqrt{2\beta\epsilon_0} e^{-(\beta/2\beta_K)a_\theta^2} \\ &\quad \times \text{Im} \left\{ e^{i(\Phi_2 - 3q/2)} \int dz \sqrt{z} \exp[-z\{1 - i\xi_2\}] I_3(a_\theta\sqrt{2z}) J_2(Qz) \right\} \end{aligned} \quad (3.13)$$

Note that since the lowest order term in $I_3(a_\theta\sqrt{2z})$ is $(a_\theta\sqrt{z})^3$, there is no echo at 4τ in the linearized dipole kick approximation.

The integrals in Eq. (3.11) and Eq. (3.13) do not appear to be analytically tractable nor do they appear to be listed in the extensive tables of integrals in [20]. However they can be evaluated numerically. As a consequence however, the optimum quadrupole strengths to maximize the echo amplitudes must be found numerically, unlike the case with the theory developed in Section 2. Detailed comparisons of the predictions from QT and DQT theories are discussed in the next section on simulations.

We briefly illustrate how the nonlinear nature of the dipole kicks changes the echo response. Fig. 2 shows the impact of increasing dipole kicks on the amplitudes of the first

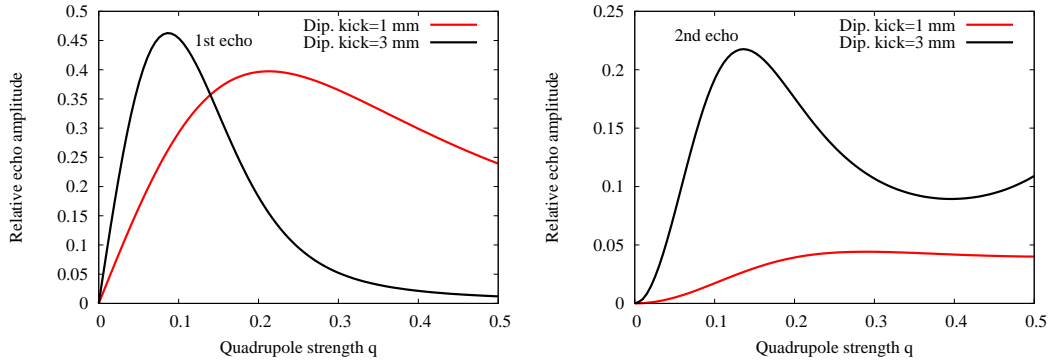


Figure 2: Left: Relative amplitude of the first echo vs quadrupole strength for two dipole kicks. Right: Relative amplitude of the second echo for the same two dipole kicks. The initial emittance is the same in both plots.

and second echoes, based on the above theory. In general we find that increasing the dipole kick lowers the optimum quadrupole kick q_{opt} and increases the relative amplitude slightly, as also seen in Section 2. On the other hand for the second echo, larger dipole kicks also decrease the corresponding q_{opt} but significantly increase its amplitude. The left plot in this figure shows the first echo's amplitude $A^{(1)}$ as a function of the quadrupole kick q for two dipole kicks at a constant beam size of 1mm. As the dipole kick increases from 1 mm to 3 mm, q_{opt} decreases while the echo amplitude at q_{opt} increases slightly. The right plot shows the response of the second echo as a function of q . At a 1 mm dipole kick, the second echo's amplitude $A^{(2)}$ has a relatively flat response to the quadrupole kick after an initial linear increase. At a 1mm kick, $A_{max}^{(2)} \sim 0.1A_{max}^{(1)}$ while at a 3mm dipole kick $A_{max}^{(2)} \sim 0.5A_{max}^{(1)}$. Increasing the dipole kick shows that $A_{max}^{(1)}(\beta_K\theta = 3 \text{ mm}) \sim 1.15A_{max}^{(1)}(\beta_K\theta = 1 \text{ mm})$ while $A_{max}^{(2)}(\beta_K\theta = 3 \text{ mm}) \sim 5A_{max}^{(2)}(\beta_K\theta = 1 \text{ mm})$, showing that the second echo is much more sensitive to the dipole kick. Summarizing, we have shown that the nonlinear dipole and quadrupole theory (DQT) removes the drawbacks of the nonlinear quadrupole theory (QT) mentioned earlier.

4 Simulations of echo amplitudes

In this section, we discuss the results of 1D echo simulations using a simple particle tracking code. The code models linear motion in an accelerator ring and nonlinear motion due to octupoles placed around the ring. A single turn dipole kick acts on the particle distribution at a chosen moment and is followed by a single turn quadrupole kick at a later time after the distribution has decohered. The beam distribution is then followed at a separate observation point for a virtual beam position monitor (BPM) and the first moment is recorded until the first few echoes have developed and then disappeared. The main beam parameters in the simulations are shown in Table 1. We do not specify the beam energy here, but note that the emittances chosen are in a range around the nominal un-normalized emittance observed during 100 GeV operation with proton beams at RHIC [14]. The octupole strengths were

Parameter	Symbol	Value
Number of particles	N_{part}	20000
Total simulation turns	-	4000 - 10,000
Tune	ν_β	0.245
Beta function at BPM, dipole, quadrupole [m]	β, β_K, β_Q	10, 10, 10
Dipole kick range [mrad]	θ	0.1 - 1.0
Quadrupole kick range	q	0.01 - 0.5
Delay time [turns]	N_τ	1400
Tune slope [1/m]	ν'	-3009

Table 1: Table of parameters

chosen to ensure a large enough nonlinear tune spread that results in decoherence times of the order of a few hundred turns but small enough that no particles were lost at the largest dipole kick used. Typically, the dipole kick was applied after 200 turns and the quadrupole kick at turn 1600. This delay time of 1400 turns is large enough so that the beam distribution had decohered completely (in most cases, but see the discussion below) at the time of the quadrupole kick. A Gaussian beam distribution in transverse (x, p) space with three seeds for each echo simulation was used and averaged to obtain the echo amplitude. The simulations were done for different initial emittances, dipole kicks and quadrupole kicks while keeping the detuning and delay parameters constant.

First, we make some general observations. The emittance growth following the dipole kick was compared with the prediction, $\varepsilon_f = \varepsilon_0[1 + \frac{1}{2}(\frac{\beta_K \theta}{\sigma_0})^2]$ and found to be within 5% of this value. Also as expected, there was no further emittance growth following the quadrupole kick. The decoherence time, calculated as the e-folding time for the centroid decay following the dipole kick, depends both on the initial emittance and on the dipole kick. We also observe that for small emittances and small dipole kicks where the decoherence time is longer than 1400 turns, the quadrupole kick was applied before the beam had completely decohered. Echoes are still observed, albeit of relatively small amplitude. These echoes have long durations that are proportional to the decoherence time; as predicted by the linear theory [17].

Figure 3 shows an example of the change in the echo pulse shape with increasing values of q , at constant emittance and constant dipole kick. We observe that as low values of q , the echo pulse is symmetric and increases in amplitude with q , but with further increase becomes asymmetric, widens, starts earlier than 2τ , then splits into two pulses of smaller amplitudes before vanishing altogether. The plots in Figure 4 show the echo pulse with increasing dipole kicks, at constant initial emittance and constant quadrupole kick. The plots in Fig. 4 also illustrate that the decoherence time decreases as the dipole kick increases. The first plot in this figure shows that an echo pulse is still formed, even though the centroid has not completely decohered at the time of the quadrupole kick.

Our goal is to maximize the echo signal by proper choices of parameters. Fig. 5 shows theory and simulations of the echo amplitude as a function of the quadrupole strength for different values of the beam emittance and the initial dipole kick. Here we will consider

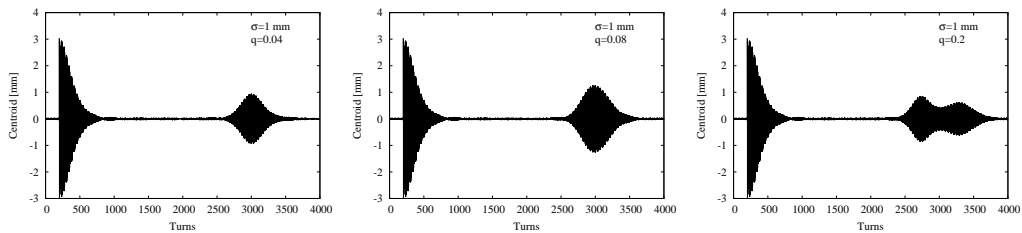


Figure 3: Time evolution of the centroid after the dipole kick at turn 200, with different strength quadrupole kicks applied at turn 1600. The echo pulse is centered around turn 3000. Both the initial emittance (corresponding to $\sigma_0 = 1$ mm at the BPM) and dipole kick = 3 mm were kept constant. Quadrupole kicks increase from left to right in the three plots. The relative amplitude of the echo has a maximum at $q = 0.08$ (center plot) at the chosen emittance.

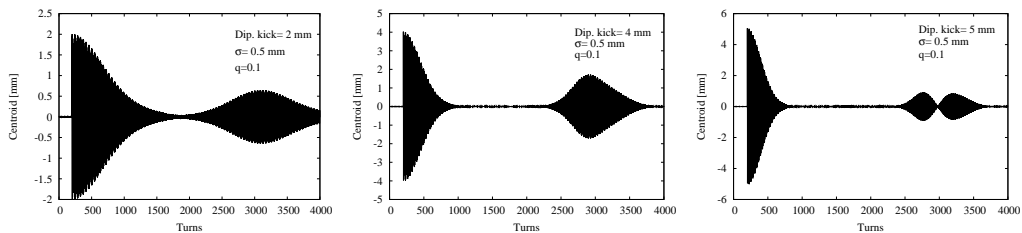


Figure 4: Centroid evolution with different dipole kicks, constant constant emittance ($\sigma = 0.5$ mm), and constant quadrupole kick $q = 0.1$. The dipole kicks increase from left to right. The decoherence time decreases with increasing dipole kick.

the simpler version of the nonlinear dipole quadrupole theory (DQT) developed in Section 3. The error bars represent the rms variation over the seeds for the initial beam distribution and are quite small in every case. First we make general comparisons between the two theories with the simulation results. The nonlinear dipole and quadrupole theory (DQT) predicts larger amplitudes than the nonlinear quadrupole theory (QT) and is usually in better agreement with the simulations. The QT predicts $A_{max} \leq 0.4$, but the DQT and the simulations show larger values of A_{max} , especially at smaller emittances. The QT predicts that the optimum q_{opt} is determined by η , the ratio of the delay to the decoherence time (see Eq. (2.42)). However the DQT predicts slightly larger values of q_{opt} than the QT, and that the echo amplitude decreases more slowly for $q > q_{opt}$. All of these predictions from DQT are in better agreement with the simulations. The differences between the theories diminish with increasing emittance. At the larger emittances studied, A_{max} in the simulations does not exceed 0.38, in agreement with the prediction of QT.

Now we turn to specific comparisons of the results shown in Fig. 5 where the initial emittance increases from top to bottom and the dipole kick increases from left to right. The top left plot in Fig. 5, shows that the simulation points are at larger amplitude than the theories. In this case the decoherence time is very long, so there is a contribution from the initial dipole kick to the centroid amplitude at the time of the echo. Consequently, the simulated echo amplitude appears to be non-zero at zero quadrupole kick. The top right plot for the larger dipole kick (3mm) shows that the peak echo amplitude from simulation lies in between the peak amplitudes from the QT and the DQT. Theoretical values of the optimum q_{opt} are close to the simulation value. However, the DQT shows a spurious oscillation for $q > 0.25$ at this low emittance. This occurs because of the oscillatory integrand and the simple numerical integration algorithm used which does not converge rapidly enough in this parameter range where both a_θ is large and $q \gg q_{opt}$. There are straightforward algorithms to improve the convergence with Bessel function integrands, see for example [22]. Such an algorithm can be implemented if required. The plots in the second and third row show that for larger emittances, both theories (especially the DQT) agree reasonably well with simulations for $q < q_{opt}$ but fall off faster with increasing q for $q > q_{opt}$ compared to the simulations. These differences may not be practically relevant, since we will use quadrupole kicks as close as possible to the optimum in experiments. In addition, the discrepancies for $a_\theta \geq 6$ may practically not matter, since it is unlikely that the beam will be kicked to amplitudes larger than 6σ , especially in hadron superconducting machines or in machines with collimator jaws placed close to this amplitude.

The plots in Fig. 6 show simulation results for the echo amplitude variation with q over a large range of dipole kicks. The left plot at the smaller initial emittance shows that at the smallest kick of 1 mm, the echo amplitude increases nearly linearly with q and A_{max} reaches a maximum value of about 0.55. As the dipole kick increases, the optimum quadrupole strength decreases, but there is little change in A_{max} . The right plot in Fig. 6 shows results at a larger initial emittance. The plots show similar behavior except that the linear response is valid over a smaller range in q . These simulation results confirm the results from theory that larger dipole kicks do not significantly impact the amplitude of the first echo.

Figure 7 shows simulation results for the variation of q_{opt} with the emittance for dipole

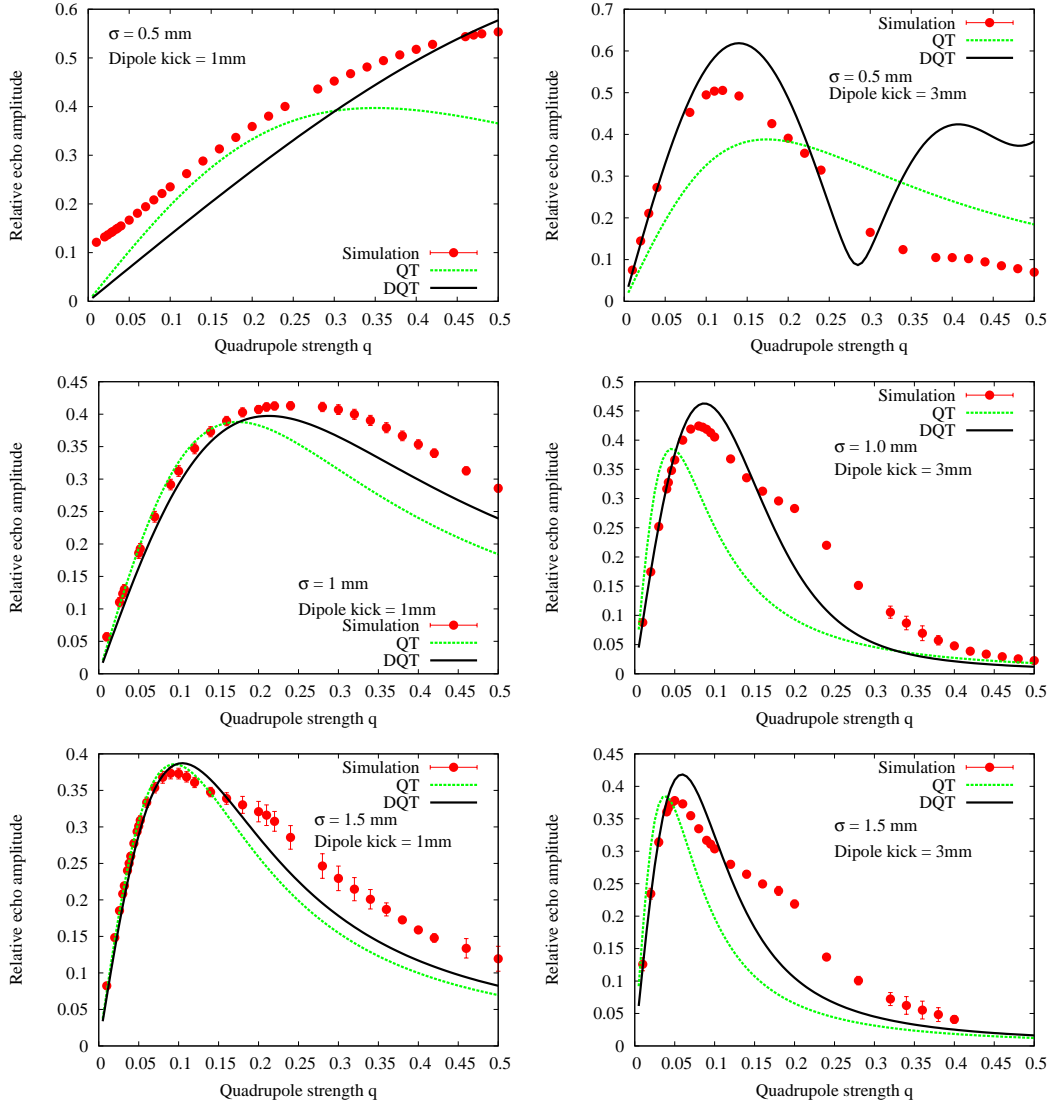


Figure 5: The relative amplitude of the first echo as a function of the quadrupole strength parameter q . Simulations (red dots) are compared with QT, the nonlinear quadrupole theory (green curve) and DQT, the nonlinear dipole-quadrupole theory (black curve). The initial emittances increase from top to bottom, at each emittance the left plot corresponds to a dipole kick= 1mm, the right plot to a dipole kick = 3 mm.

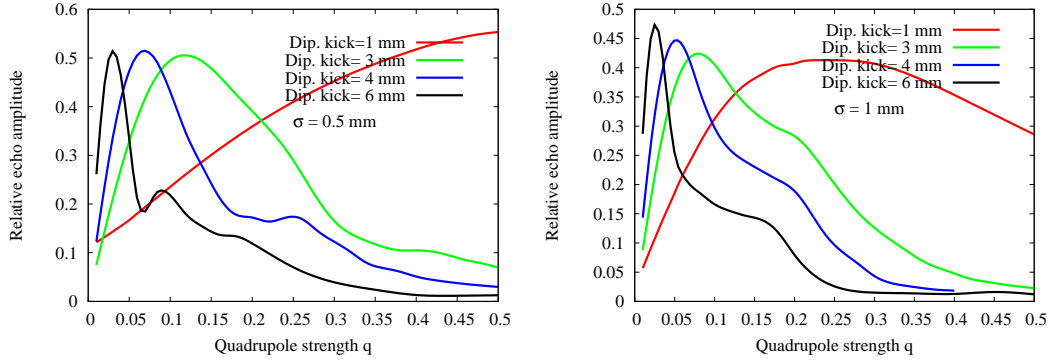


Figure 6: Relative echo amplitude vs the quadrupole strength from simulations for different dipole kicks. Left: Initial beam size at the BPM $\sigma = 0.5$ mm; Right: $\sigma = 1$ mm. In both plots the maximum echo amplitude is not significantly affected by increasing the dipole kick, but the value of q_{opt} changes significantly.

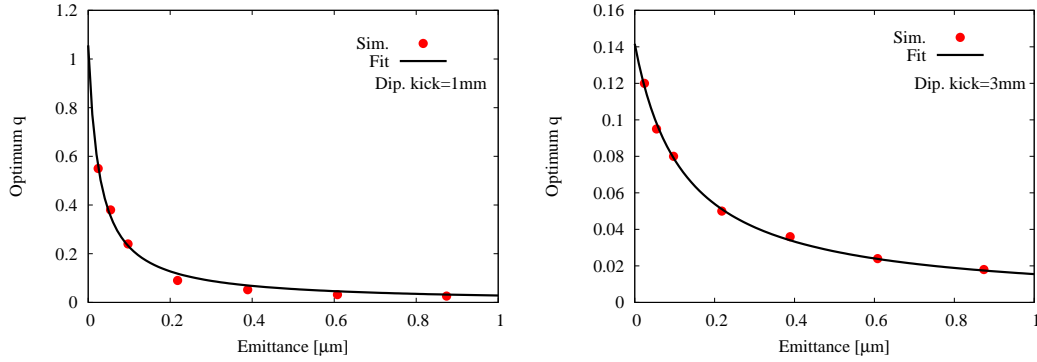


Figure 7: Optimum quadrupole strength as a function of the initial emittance for two initial dipole kicks: simulations (red dots) compared with fits to the form in Eq. (4.1).

kicks of 1mm and 3mm. At the larger dipole kick, q_{opt} values are about an order of magnitude smaller over most of this range of emittances, except at the largest emittances. The plots in Fig. 7 also show a fit to a function

$$q_{opt}(\epsilon_0) = \frac{a_q}{\epsilon_0 + b_q} \quad (4.1)$$

where (a_q, b_q) are fit parameters. This fit function models the variation of q_{opt} quite well in all the cases studied.

The DQT theory in Section 3 had shown that A_{max} is determined by the emittance and the relative dipole kick a_θ , when the delay τ and detuning are kept constant. The left plot in Fig. 8 shows simulation results for A_{max} as a function of the initial beam size σ_0 , while the right plot shows A_{max} as a function of a_θ . We find that A_{max} as a function of σ_0 is best fit by a functional form

$$A_{max}(\sigma_0) = \frac{a}{\sigma_0 + b} \quad (4.2)$$

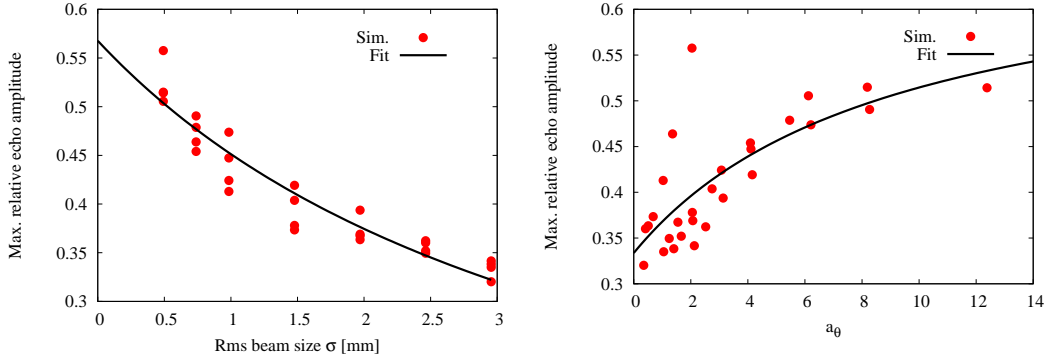


Figure 8: Maximum relative echo amplitude A_{max} as a function of the beam size (left plot) and the relative dipole kick (right plot)

where (a, b) are fit parameters. It follows that the maximum possible relative echo amplitude at vanishingly small emittance is $A_{asyp,\sigma} \equiv A_{max}(\sigma \rightarrow 0) = a/b$. On the other hand, A_{max} as a function of a_θ is well fit by a rational function of the form

$$A_{max}(a_\theta) = \frac{pa_\theta + q}{a_\theta + s} \quad (4.3)$$

where (p, q, s) are fit parameters. This function predicts that at very large a_θ , the asymptotic value is given by $A_{asyp,a_\theta} \equiv A_{max}(a_\theta \rightarrow \infty) = p$. The plots in Fig. 8 show the best fits to these functional forms. While there are the same number of simulation points in both plots, the scatter of points around the best fit is much smaller in the left plot. The asymptotic values predicted by the two fits are $A_{asyp,\sigma} = 0.57$ and $A_{asyp,a_\theta} = 0.68$. The value of $A_{asyp,\sigma}$ is much closer to the largest value seen in the simulations while reaching the value of A_{asyp,a_θ} may require unrealistically large values of the dipole kick. These results again confirm that the maximum echo is largely determined by the initial beam emittance; the variation with dipole kick at a given emittance is within 15% over the dipole kicks shown. A test beam with the smallest feasible emittance and modest dipole kick $a_\theta \sim 1$ may suffice to maximize the relative echo amplitude. While the absolute echo amplitudes increase with the dipole kick, amplitudes ≥ 0.1 mm can be measured accurately when BPM resolutions are of the order of tens of microns. However, the advantage of a larger dipole kick, as seen in Fig. 7 is that the optimum quadrupole strength is smaller, by up to an order of magnitude depending on the emittance. In general, smaller dipole kicks are to be preferred since they are less likely to lead to beam loss. In practice, generating the largest amplitude echo may require a compromise between the largest dipole kick tolerable and quadrupole kick strengths achievable. Studies of stimulated echoes (not discussed here) show that a single large quadrupole kick can be replaced by a few lower strength quadrupole kicks, spaced apart in time depending on the tune.

4.1 Multiple Echoes

Multiple echoes could be useful to observe for the information they may provide about the machine and beam, such as diffusion and nonlinearities. It is also possible to enhance the

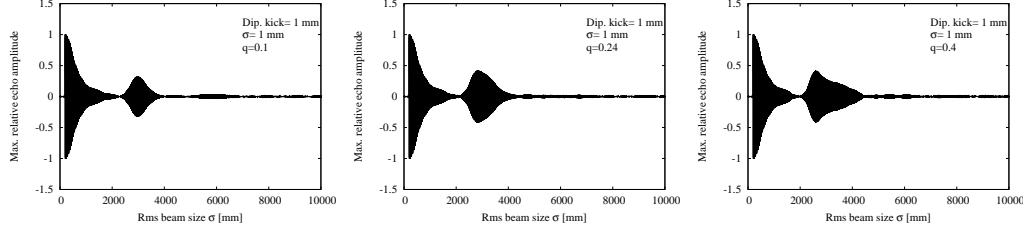


Figure 9: Multiple echoes at constant emittance, quadrupole kick and increasing values of the dipole kick strength, left to right. The second echo (centered at turn 5800) and third echo (centered at turn 8600) become visible at the larger dipole strengths.

Dipole kick[mm]	Quad. strength q	1st echo amplitude		2nd echo amplitude	
		Theory	Simulation	Theory	Simulation
1.0	0.24	0.39	0.42	0.04	0.024
3.0	0.08	0.45	0.42	0.15	0.13
4.0	0.052	0.48	0.45	0.17	0.16
6.0	0.026	0.49	0.47	0.17	0.18

Table 2: Maximum relative amplitudes of the first and second echoes from theory and simulations. The emittance is constant at $\epsilon_0 = 9.7 \times 10^{-8}$ m or rms size $\sigma_0 = 1$ mm. For each dipole kick, the quadrupole strength is chosen from simulations that maximizes the first echo amplitude.

multiple echoes with different sequences of quadrupole pulses (stimulated echoes), so it is of interest to quantify their amplitudes with just the single quadrupole kick studied in this paper. They were also observed during the echo experiments at RHIC [14].

Simulations with 10,000 turns are sufficient to observe up to the third echo (if it exists) when the delay τ between the dipole and quadrupole kicks is 1400 turns. We find that increasing the quadrupole strength influences only the first echo but has no influence on the later echoes which do not exist at small dipole kicks. The plots in Fig. 9 show the evolution of the centroid at constant emittance and constant quadrupole kick but increasing dipole kick. In this case, only the first echo is seen at 1 mm kick, the second echo is visible at a 3 mm kick while at a 6 mm kick, both the second and third echoes are observed, with comparable amplitudes.

Table 2 compares the maximum relative amplitudes of the first and second echoes from theory and simulations at a constant emittance. The quadrupole strength was chosen such that it led to the largest amplitude of the first echo. In most cases, theory and simulation results for the maximum amplitude are within 10%. The only exception is the case with the second echo at the smallest dipole kick of 1 mm; these amplitudes are very small in both theory and simulations. We also observe in the simulations that at $q = q_{opt}$ for the first echo, the second echo has started to bifurcate into two pulses, so values of $q < q_{opt}$ would be more suitable for the optimal second echo. Simulations also validate the theoretical result from DQT that the amplitudes of the second and later echoes increase significantly

with the dipole kick.

5 Spectral analysis of the echo pulse

The time dependent echo pulse shows that the amplitude is modulated at a frequency shifted from the betatron frequency. In the completely linear theory [17] and Eq. (2.41) in Section 2, the time dependent pulse is $\langle x(t) \rangle = \beta_K \theta Q A_F(t)$ where

$$A_F(t) = \frac{1}{(1 + \xi(t)^2)^{3/2}} \sin[\Phi + 3\Theta(t)], \quad \Phi = \omega_\beta(t - 2\tau), \quad \Theta = \text{Arctan}[\xi(t)] \quad (5.1)$$

Since $\xi(t) = \omega' \varepsilon_0(t - 2\tau)$, the lattice nonlinearity parameter ω' can be retrieved from the frequency spectrum. Taking the Fourier transform,

$$\tilde{A}_F(\omega) = \int_{-\infty}^{\infty} dt e^{i\omega t} A_F(t) = \frac{1}{2i} \int_{-\infty}^{\infty} dt e^{i\omega t} \frac{1}{(1 + \xi^2)^{3/2}} \left[e^{i(\Phi+3\Theta)} - e^{-i(\Phi+3\Theta)} \right]$$

The first term contributes to the negative frequency spectrum while the second contributes to the positive frequency part. Considering the second term

$$\tilde{A}_F(\omega > 0) = -\frac{1}{2i} e^{2i\omega_\beta \tau} \int_{-\infty}^{\infty} dt e^{i(\omega - \omega_\beta)t} \frac{1}{(1 + \xi^2)^{3/2}} e^{-3i\Theta}$$

This can be evaluated by a contour integration method, see Appendix B. The result for the echo spectrum as a function of frequency is

$$\tilde{A}_F(\omega) = \begin{cases} -\frac{\pi}{6} \frac{e^{i2(\omega - \omega_\beta)\tau}}{\mu \omega_{rev}} \delta^3 e^{-\delta}, & \delta \geq 0 \\ 0, & \delta < 0 \end{cases} \quad (5.2)$$

$$\delta \equiv \frac{\omega - \omega_\beta}{\mu \omega_{rev}} = \frac{\nu - \nu_\beta}{\mu} \quad (5.3)$$

where $\mu = \omega' \varepsilon / \omega_{rev}$ is the tune shift at the rms beam size. This result shows first that the spectrum is non-zero only on one side of the nominal tune ν_β : above ν_β if $\mu > 0$ or below ν_β if $\mu < 0$. It also follows that the non-zero part of the spectrum has a peak at $\delta = 3$ or at a tune given by

$$\nu_{peak} = \nu_\beta + 3\mu \quad (5.4)$$

One measure of the width of the spectrum is the full width at half maximum (FWHM), which we find numerically to be $\delta_{FWHM} = 4.13$. Hence in tune space, the FWHM is

$$\Delta \nu_{FWHM} = 4.13\mu \quad (5.5)$$

Thus both the tune of the echo pulse as well as the width of the echo spectrum are related to the detuning. From the uncertainty relation for Fourier transforms $\Delta t \Delta \omega \geq 1/2$ and using the FWHM for the echo pulse in time [17, 15], $\Delta t_{FWHM} = 1.53/(\omega_{rev}\mu)$, we expect that

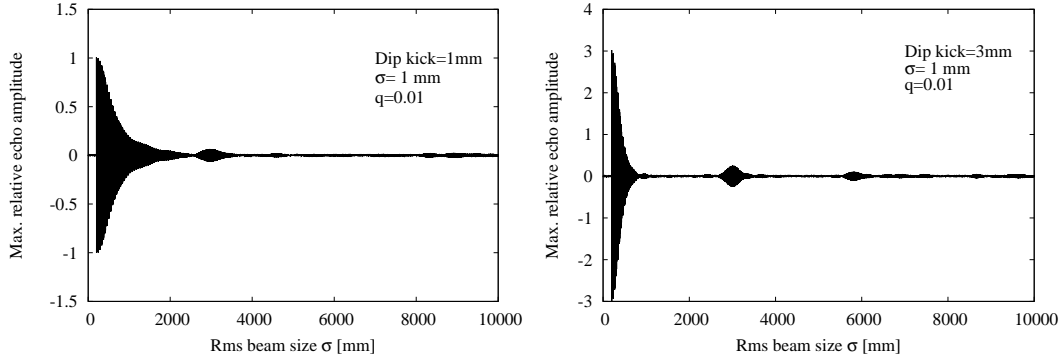


Figure 10: Left: Tune shifts (without echoes) vs the emittance. The emittance was changed by varying dipole kicks. Also shown is the straight line fit which yields the tune slope parameter ν' . Right: Spectra without echo and with echoes. The spectrum without an echo was obtained with $q = 0$ while the echo spectra were obtained with the same dipole kick (1 mm), the same value of $q = 0.01$ and two initial emittances corresponding to $\sigma_0 = 1.5$ mm and $\sigma_0 = 2$ mm. The vertical dashed line shows the bare lattice tune.

$\Delta\nu \geq \mu/3.06$. If we interpret the FWHM as a measure of the uncertainty (although the rms spread is the usual measure), then Eq. (5.5) satisfies the uncertainty relation.

The tune shift itself can be calculated simply from the time derivative of the phase $\Phi + 3\Theta$ and assuming that $\text{Arctan}[\xi] \approx \xi = \omega'\epsilon_0(t - 2\tau)$ which is valid near the center of the echo at $t = 2\tau$. This yields $\omega \approx \omega_\beta + 3\omega'\epsilon_0$, the same as the exact result. The additional advantage of the Fourier transform is that we also obtain the echo spectrum shape and width.

The echo spectrum can also be calculated in the linear dipole kick and nonlinear quadrupole kick regime, when the time dependent echo pulse is given by Eq. (2.39). It has the same form as that in the completely linear regime, the time dependent phase shift from the betatron phase Φ_β is again $3\Theta(t)$ where now Θ is given by Eq. (2.31). Using the same approximation of a small argument of the Arctan function, we have for the angular betatron frequency shift

$$\Delta\omega = 3\frac{d}{dt}\Theta \approx 3\frac{d}{dt}\left[\frac{\xi}{1 - \xi^2 + Q^2}\right] \approx 3\frac{\omega'\epsilon}{1 + Q^2} \quad (5.6)$$

where we assumed $\xi \ll 1$ in the denominator and included the contribution of the dipole kick to the emittance. Thus the nonlinearity of the quadrupole kick will reduce the tune shift by a small amount from the linear regime, assuming $Q^2 < 1$.

5.1 FFT of the echo pulse

Here we use the simulation code to calculate the spectrum of the echo pulse and compare the results with the theory developed above. One way of measuring the detuning parameter is to kick the beam to a range of amplitudes with varying dipole strengths. Each dipole kick excites the beam to a different emittance allowing the betatron tune to be measured

Final emittance ε [μm]	Theoretical $\Delta\nu$ $\Delta\nu = 3\nu'\varepsilon$	Simulated $\Delta\nu$
0.27	-0.0024	-0.0023
0.35	-0.0031	-0.0028
0.44	-0.0039	-0.0038
0.54	-0.0049	-0.0043
0.65	-0.0059	-0.0057

Table 3: Example of using the echo spectrum to measure the detuning, using a small amplitude dipole kick. All the echoes were generated with the same dipole kick of 1 mm and the same quadrupole kick $q = 0.01$. The final un-normalized emittance is shown in the first column. In all cases, the emittance increased by $\Delta\varepsilon = 0.05 \mu\text{m}$. The second and third columns show the theoretical and simulated tune shifts respectively. The value of $\nu' = -3009 /\text{m}$ was found using the simulation shown in the left plot of Fig. 10

as a function of emittance. The left plot in Figure 10 shows an example in our case. Here the quadrupole kick was set to zero so that no echoes are excited and the initial emittance ($\sigma_0 = 1 \text{ mm}$) was kept constant. Dipole kicks over a range of 0.5-10 mm were used to vary the final emittance. Using the centroid data around the time of the echo formation for the FFT analysis ensures that the beam has decohered to its asymptotic emittance. As expected the tune shifts in this plot lie on a straight line and yield the tune slope as $\nu' = dv/d\varepsilon = -3009 \text{ m}^{-1}$. The right plot shows spectra with and without echoes from an analysis of the centroid data using 1024 turns centered at the first echo. The spectra with echoes are shown for two initial emittances and the same dipole kick of 1 mm. The beam is kicked to the same amplitude, but as the theory predicts, the negative detuning parameter causes the echo spectrum to shift to the left and the spectrum widens with increasing initial emittance. Table 3 shows a comparison of the simulated tune shifts and the theoretical value expected from the analysis above. The prerequisites for using the echo spectrum to measure the detuning are that the initial beam decoherence must have a negligibly small contribution to the echo, the echo pulse should be without distortions and obtained with small dipole and quadrupole kicks so that the linear analysis is valid. Simulations of the echo spectrum at larger quadrupole strengths show that the echo tunes are not significantly affected, as expected from the analysis above. These results show that with some care, the echo spectrum can be used to measure the nonlinear detuning parameter without large amplitude dipole kicks.

6 Conclusions

In this paper we developed theories of one dimensional transverse beam echoes that are nonlinear in the dipole and quadrupole kick strength parameters with the goal of maximizing the echo amplitudes. Other relevant parameters are the initial beam emittance ε_0 , the frequency slope with emittance ω' and the delay τ between the dipole and quadrupole kicks.

The simpler theory (QT), is linear in the dipole strength but nonlinear in the quadrupole strength q . This theory yields simple expressions for the optimum quadrupole strength q_{opt} and the time dependent echo response. The optimum quadrupole strength is shown to decrease as the initial emittance and dipole kick strength increase. This theory predicts that for emittances large enough that the decoherence time $\tau_D \ll \tau$, the maximum echo amplitude relative to the dipole kick amplitude $A_{max} \approx 0.4$. Among the drawbacks of QT are that it does not include ab initio the emittance growth due to the dipole kick, but has to be included as a correction. Nor does it predict the occurrence of echoes at multiples of 2τ beyond the first echo at 2τ . The second theory (DQT), which is nonlinear in both kicks, removes these drawbacks. The disadvantage is that it results in more complicated expressions for the echo amplitude that require numerical integration. This theory predicts larger amplitude echoes than those with QT. It also shows that increasing the dipole kick strength can reduce q_{opt} by an order of magnitude but has a minor influence on the relative amplitude of the first echo. However the amplitudes of later echoes at $4\tau, 6\tau, \dots$ increase significantly with the dipole kick.

One of the first observations from accompanying simulations was that τ_D decreases with increasing either the initial emittance or dipole kick. We found that at fixed detuning and delay, A_{max} of the first echo increases with smaller emittances but has a weak dependence on the dipole kick, in agreement with theory. In the limit of vanishing emittance $\lim_{\epsilon_0 \rightarrow 0} A_{max} = 0.57$ (see Fig. 8). Both the QT and DQT are in good agreement with the simulations for dipole kicks $\sim \sigma_0$, the initial rms beam size. As a function of q , the echo amplitude from DQT was in reasonable agreement with simulations for dipole kicks $\leq 5\sigma_0$. For even larger larger dipole kicks, DQT yields acceptable results when $q \leq q_{opt}$ but diverges from simulations for $q \gg q_{opt}$. We attribute this to artifacts in the numerical integration which can be corrected. Machine protection issues will forbid large dipole kicks, so in practice DQT should be useful for estimating the echo amplitude. The simulations showed that the optimum quadrupole strength for higher order echoes changes with the echo order. Amplitudes of the later echoes increased with the dipole kick, again in accordance with the theory. The maximum amplitudes of the first and second echoes from theory and simulations agreed well, up to the largest dipole kick (6σ) tested. These results suggest that a strategy for enhancing the echo signal would be to use a pencil beam with reduced emittance, by scraping with collimators for example, (but with sufficient intensity to trigger the BPMs) and dipole kicks $\sim \sigma_0$. The quadrupole strength should be scanned in a range around q_{opt} for the first echo to maximize its amplitude. If multiple echoes are not observed initially, increasing the dipole kick strength in incremental steps and rescanning around the appropriate q_{opt} should reveal their presence.

Spectral analysis of the echo pulse showed that the tune of the pulse is shifted from the bare betatron tune by 3μ where μ is the tune shift at the rms size. This was confirmed with simulations using small amplitude dipole and quadrupole kicks. This suggests that the echo pulses generated with small dipole kicks could be used to measure the detuning without the necessity of kicking the beam over a large range of amplitudes.

Acknowledgments

We thank the Lee Teng summer undergraduate program at Fermilab for awarding an internship to Yuan Shen Li in 2016. Fermilab is operated by the Fermi Research Alliance, LLC under U.S. Department of Energy contract No. DE-AC02-07CH11359.

Appendices

A Appendix: Complete theory of nonlinear dipole and quadrupole kicks

Here we consider the complete distribution function (DF) following the dipole kick without the simplifying approximations made in Section 3. Using the notation from this section and keeping terms to $O(q)$, the DF at time τ after the dipole kick,

$$\begin{aligned} \psi_5(z, \phi, t) = & \frac{1}{2\pi\epsilon_0} \exp\left[-\frac{\beta_K \theta^2}{2\epsilon_0}\right] \exp\left\{-\frac{1}{\epsilon_0} [z\epsilon_0(1 - q \sin 2\phi_{-\Delta\phi}) \right. \\ & \left. + \beta_K \theta \sqrt{\frac{2\epsilon_0 z}{\beta}} \left(1 - \frac{1}{2}q \sin 2\phi_{-\Delta\phi}\right) \sin(\phi_{-\Delta\phi} - \tau\omega(z) - q \cos^2 \phi_{-\Delta\phi} + Qz \sin 2\phi_{-\Delta\phi})] \right\} \end{aligned} \quad (\text{A.1})$$

We define dimensionless parameters

$$a_\theta = \frac{\beta_K \theta}{\sigma_0}, \quad b_1 = q, \quad b_2 = \sqrt{2}a_\theta, \quad b_3 = \frac{\sqrt{2}}{4}qa_\theta, \quad b_i \geq 0 \quad (\text{A.2})$$

We have the following ordering hierarchy assuming $q \ll 1, a_\theta \sim O(1)$

$$b_2 > (b_1, b_3), \quad b_3 > b_1 \text{ if } a_\theta > 2\sqrt{2}$$

In the theory developed in Section 3, we had kept only b_2 and dropped b_1, b_3 .

We have for the dipole moment

$$\langle x(t) \rangle = \frac{\sqrt{2\beta\epsilon_0}}{2\pi} \exp\left[-\frac{\beta_K \theta^2}{2\epsilon_0}\right] \int dz \sqrt{z} \exp[-z] T_\phi(z) \quad (\text{A.3})$$

$$\begin{aligned} T_\phi(z) \simeq \text{Re} \left\{ \int d\phi e^{i\phi} \exp \left[b_1 z \sin(2\phi_{-\Delta\phi}) - b_2 \sqrt{z} \sin(\phi_{-\Delta\phi} - \frac{1}{2}q - \tau\omega + Qz \sin 2\phi_{-\Delta\phi}) \right. \right. \\ \left. \left. + b_3 \sqrt{z} \cos \left(\phi_{-\Delta\phi} + \frac{1}{2}q + \tau\omega - Qz \sin 2\phi_{-\Delta\phi} \right) \right. \right. \\ \left. \left. - b_3 \sqrt{z} \cos \left(3\phi_{-\Delta\phi} - \frac{1}{2}q - \tau\omega + Qz \sin 2\phi_{-\Delta\phi} \right) \right] \right\} \end{aligned} \quad (\text{A.4})$$

where we used the approximation in Eq.(2.14). Using the generating function expansions

for the modified Bessel functions, we have

$$T_\phi(z) = \text{Re} \left\{ \sum_{k_1} \sum_{k_2} \sum_{k_3} \sum_{k_4} i^{k_1+k_2} (-1)^{k_4} I_{k_1}(b_1 z) I_{k_2}(b_2 \sqrt{z}) I_{k_3}(b_3 \sqrt{z}) I_{k_4}(b_3 \sqrt{z}) \right. \\ \times \exp[i(k_1 2\Delta\phi - k_2(\Delta\phi + \tau\omega + q/2) - k_3(\Delta\phi - \tau\omega - q/2) \\ \left. - k_4(3\Delta\phi + \tau\omega + q/2))] \right. \\ \left. \int d\phi \exp[i([1 - 2k_1 + k_2 + k_3 + 3k_4]\phi + (k_2 + k_4 - k_3)Qz \sin 2\phi - \Delta\phi)] \right\}$$

We expand into a Bessel function, integrate over ϕ , replace k_2 by $2k_1 - k_3 - 3k_4 - 2l - 1$, and drop the sum over k_2 . After simplifying the phase factor, the integrated term is

$$T_\phi(z) = 2\pi \text{Re} \left\{ \sum_{k_1} \sum_{k_3} \sum_{k_4} \sum_l i^{k_1-k_3+k_4-1} (-1)^{k_1+k_4+l} \exp[i - \frac{1}{2}q([2(k_1 - k_3 - k_4 - l) - 1])] \right. \\ I_{k_1}(b_1 z) I_{2k_1-k_3-3k_4-2l-1}(b_2 \sqrt{z}) I_{k_3}(b_3 \sqrt{z}) I_{k_4}(b_3 \sqrt{z}) J_l([2(k_1 - k_3 - k_4 - l) - 1]Qz) \\ \left. \times \exp(i[\omega(t - 2\tau(k_1 - k_3 - k_4 - l))]) \right\}$$

Since the amplitude is locally maximum when the phase factor vanishes, the form above shows that echoes occur at close to the times t when $t - 2\tau(k_1 - k_3 - k_4 - l) = 0$. As expected, this predicts echoes only at times close to multiples of 2τ . We replace $k_1 - k_3 - k_4 - l = n$, which leads to

$$T_\phi(z) = 2\pi \text{Im} \left\{ \sum_{k_1} \sum_{k_3} \sum_{k_4} \sum_n i^{k_1-k_3+k_4} (-1)^{k_1+k_4+n} \exp[-i\frac{1}{2}q(2n-1)] \right. \\ I_{k_1}(b_1 z) I_{k_3-k_4+2n-1}(b_2 \sqrt{z}) I_{k_3}(b_3 \sqrt{z}) I_{k_4}(b_3 \sqrt{z}) J_{k_1-k_3-k_4-n}([2n-1]Qz) \\ \left. \times \exp(i[\omega(t - 2n\tau)]) \right\}$$

Using the phase variables Φ_n, ξ_n defined earlier in Section 3, we can write the complete expression for the dipole moment as (after replacing $k_3 \rightarrow k_2, k_4 \rightarrow k_3$)

$$\langle x(t) \rangle = \sqrt{2\beta\epsilon_0} \exp[-\frac{\beta_K \theta^2}{2\epsilon_0}] \text{Im} \left\{ \int dz \sqrt{z} \exp[-\{1 - i\xi_n\}z] \right. \\ \sum_n \sum_{k_1} \sum_{k_2} \sum_{k_3} i^{k_1-k_2+k_3} (-1)^{k_1+k_3+n} e^{i[\Phi_n - \frac{1}{2}q(2n-1)]} \\ \left. I_{k_1}(b_1 z) I_{k_2-k_3+2n-1}(b_2 \sqrt{z}) I_{k_2}(b_3 \sqrt{z}) I_{k_3}(b_3 \sqrt{z}) J_{k_1-k_2-k_3-n}([2n-1]Qz) \right\} \quad (\text{A.5})$$

This is the most general form of the time dependent echo. To recover the approximate theory of Section 3, we put $b_1 = 0 = b_3$. Since $I_0(0) = 1, I_{m \neq 0}(0) = 0$, this requires $k_1 = 0 = k_2 = k_3$. Using $J_{-n}(z) = (-1)^n J_n(z)$, we recover the same expression as in Eq.3.10). In the limiting case of no dipole kick, then $b_2 = 0 = b_3$ and using the same Bessel function properties, we find that the dipole moment vanishes, as it should. In the other limiting case of no quadrupole kick, we have $b_1 = b_3 = Q = 0$ and we have a non-zero contribution only

with $k_1 = k_2 = k_3 = n = 0$ and we have

$$\begin{aligned}\langle x(t) \rangle_{q=0} &= \sqrt{2\beta\epsilon_0} \exp\left[-\frac{\beta_K\theta^2}{2\epsilon_0}\right] \text{Im} \left\{ e^{i\omega\beta t} \int dz \sqrt{z} \exp[-\{1 - i\omega'\epsilon_0 t\}z] I_1(b_2\sqrt{z}) \right\} \\ &= \beta_K\theta \text{Im} \left\{ \frac{e^{i\omega\beta t}}{(1 - i\omega'\epsilon_0 t)^2} \exp\left[\frac{\beta_K\theta^2}{2\epsilon_0} \frac{i\omega'\epsilon_0 t}{(1 - i\omega'\epsilon_0 t)}\right] \right\}\end{aligned}\quad (\text{A.6})$$

The last expression is the same as that derived by earlier authors [18, 17].

Returning to the general case with non-zero dipole and quadrupole kicks, we extract the dominant terms contributing to the first and second echoes at 2τ and 4τ , by setting $n = 1$ and $n = 2$ respectively in Eq. (A.5),

$$\begin{aligned}\langle x(2\tau) \rangle &\simeq \sqrt{2\beta\epsilon_0} \exp\left[-\frac{\beta_K\theta^2}{2\epsilon_0}\right] \text{Im} \left\{ \int dz \sqrt{z} \exp[-\{1 - i\xi_1\}z] \right. \\ &\quad \sum_{k_1=-N_1}^{N_1} \sum_{k_2=-N_2}^{N_2} \sum_{k_3=-N_3}^{N_3} i^{k_1-k_2+k_3} (-1)^{k_1+k_3+1} e^{i[\Phi_1 - \frac{1}{2}q]} \\ &\quad \left. I_{k_1}(b_1z) I_{k_2-k_3+1}(b_2\sqrt{z}) I_{k_2}(b_3\sqrt{z}) I_{k_3}(b_3\sqrt{z}) J_{k_1-k_2-k_3-1}(Qz) \right\}\end{aligned}\quad (\text{A.7})$$

$$\begin{aligned}\langle x(4\tau) \rangle &\simeq \sqrt{2\beta\epsilon_0} \exp\left[-\frac{\beta_K\theta^2}{2\epsilon_0}\right] \text{Im} \left\{ \int dz \sqrt{z} \exp[-\{1 - i\xi_2\}z] \right. \\ &\quad \sum_{k_1=-N_1}^{N_1} \sum_{k_2=-N_2}^{N_2} \sum_{k_3=-N_3}^{N_3} i^{k_1-k_2+k_3} (-1)^{k_1+k_3} e^{i[\Phi_2 - \frac{3}{2}q]} \\ &\quad \left. I_{k_1}(b_1z) I_{k_2-k_3+3}(b_2\sqrt{z}) I_{k_2}(b_3\sqrt{z}) I_{k_3}(b_3\sqrt{z}) J_{k_1-k_2-k_3-2}(3Qz) \right\}\end{aligned}\quad (\text{A.8})$$

Here the summations are written to indicate that a finite number of terms are calculated. From Eq. (A.8), it is easily checked that there is no contribution to the echo at 4τ from terms linear in the dipole kick. This confirms the result in Section 2 where the analysis to first order in the dipole kick did not reveal the presence of multiple echoes.

The convergence of the above expansions is rapid when the dipole kick parameter a_θ is sufficiently small. For large $a_\theta \gg 1$, which can happen with either a large dipole kick or small emittance or both, the above expansions do not converge rapidly enough to be usable in some instances. A different approach would be to use the smallness of the parameter $b_1 \ll 1$ to expand $\exp[b_1z \sin[2(\phi - \Delta\phi) - q/2]]$ in Eq. (A.4) into a power series in b_1 instead. A similar approach had been used in [23] in calculating beam-beam tune shifts due to long-range interactions and was found to converge rapidly. We will not investigate this method further here. For the comparisons with simulations, we use the equations Eq. (A.7) and (A.8) above when they do converge rapidly and in other cases, use the more approximate version developed in Section 3.

B Appendix: Echo Spectrum by Fourier transform

Consider the Fourier amplitude from Section 5

$$\tilde{A}_F(\omega > 0) = -\frac{1}{2i} e^{2i\omega\beta\tau} \int dt e^{-i(\omega - \omega_\beta)t} \frac{1}{(1 + \xi^2)^{3/2}} e^{-3i\Theta} \equiv e^{2i\omega\beta\tau} I(\omega) \quad (\text{B.1})$$

Using

$$\text{Arctan}[x] = \frac{i}{2} \ln\left[\frac{1-ix}{1+ix}\right]$$

and the definition of $\Theta = \text{Arctan}[\xi(t)]$, we have

$$\exp[-i3\Theta(t)] = i \frac{(\xi+i)^3}{(1+\xi^2)^{3/2}}$$

Hence the integral reduces to

$$I(\omega) = i \int_{-\infty}^{\infty} dt e^{-i(\omega-\omega_\beta)t} \frac{1}{(\xi-i)^3} = \frac{i}{\mu\omega_{rev}} e^{-i((\omega-\omega_\beta)2\tau)} \int_{-\infty}^{\infty} d\xi \frac{e^{i\delta\xi}}{(\xi-i)^3} \quad (\text{B.2})$$

where we defined $\delta = (\omega - \omega_\beta)/(\mu\omega_{rev})$ and $\mu\omega_{rev} = \omega'\varepsilon$. Complexifying $\xi \rightarrow z$ we consider the contour integral $\oint dz e^{i\delta z}/(z-i)^3$ over a semi-circular contour with the radius at infinity. If $\delta > 0$, then we consider the positive half plane and the integral vanishes over the arc leaving only the contribution over the real axis. The integrand has third order poles at $z = i$, hence

$$\begin{aligned} \int_{-\infty}^{\infty} dz \frac{e^{i\delta z}}{(z-i)^3} &= \oint_C dz \frac{e^{i\delta z}}{(z-i)^3} = 2\pi i \times \text{Residue}\left[\frac{e^{i\delta z}}{(z-i)^3}\right]_{z=i} \\ &= \frac{\pi}{3} \delta^3 e^{-\delta}, \quad \delta > 0 \end{aligned} \quad (\text{B.3})$$

On the other hand if $\delta < 0$, we consider the lower half plane where again the contribution from the arc vanishes. However the integrand is analytic over the lower half plane, hence the contour integral vanishes. Thus we have

$$\int_{-\infty}^{\infty} dz \frac{e^{i\delta z}}{(z-i)^3} = 0, \quad \delta < 0 \quad (\text{B.4})$$

Hence the Fourier integral for positive frequencies, after combining Eqs. (B.1), (B.2) and the above contour integrations, is

$$\begin{aligned} \tilde{A}_F(\omega > 0) &= -\frac{\pi}{6\mu\omega_{rev}} e^{-i(\omega-2\omega_\beta)2\tau} \delta^3 e^{-\delta}, \quad \delta \geq 0 \\ &= 0, \quad \delta < 0 \end{aligned} \quad (\text{B.5})$$

The echo spectrum is determined by the Fourier amplitude $|\tilde{A}_F(\omega)| = (\pi/(6\mu\omega_{rev}))\delta^3 e^{-\delta}$ for $\omega \geq \omega_\beta$ and vanishes for $\omega < \omega_\beta$, assuming $\mu > 0$ while the converse is true if $\mu < 0$.

References

- [1] E.I. Hahn, *Spin Echoes*, *Phy. Rev.* **80**, 580 (1950)
- [2] B.M. Dale, M.A. Brown and R.C. Semelka, *MRI: Basic Principles and Applications*, Wiley Blackwell (2015)

- [3] N.A. Kurnit, I.D. Abella and S.R. Hartmann, *Observation of a Photon Echo*, Phys. Rev. Lett. **13**, 567 (1964)
- [4] R.W. Gould, T.M. O’Neil and J.H. Malmberg, , *Plasma Wave Echo*, Phys. Rev. Lett. **19**, 219 (1967)
- [5] J.H. Malmberg, C.B. Wharton, R.W. Gould and T.M. O’Neil, *Observation of Plasma Wave Echoes*, Phys. Fluids, **11**, 1147 (1968)
- [6] M.F. Andersen, A.Kaplan and N. Davidson, *Echo Spectroscopy and Quantum Stability of Trapped Atoms*, Phys. Rev. Lett., **90**, 023001 (2003)
- [7] J.H. Yu, C.F. Driscoll and T.M. O’Neil, *Phase mixing and echoes in a pure electron plasma*, Phys. Plasmas, **12**, 055701 (2005)
- [8] G. Karras, E. Hertz, F. Billard, B. Lavorel, J.-M. Hartmann, O. Faucher, Erez Gershnel, Yehiam Prior, and Ilya Sh. Averbukh, *Orientation and Alignment Echoes*, Phys. Rev. Lett. **114**, 153601 (2015)
- [9] G.V. Stupakov, Preprint, SSCL-579 (1992)
- [10] G. V. Stupakov and S.K. Kaufmann, Preprint SSCL-587 (1992)
- [11] L.K. Spentzouris, J-F. Ostiguy, P.L. Colestock, *Measurement of Diffusion Rates in High Energy Synchrotrons using Longitudinal Beam Echoes*, Phys. Rev. Lett., **76**, 620 (1996)
- [12] O. Bruning, T. Linnecar, F. Ruggiero, W. Scandale, E. Shaposhnikova, D. Stellfeld, *Beam Echoes in the CERN SPS*, Proceedings of PAC97, 1816 (1997)
- [13] G. Arduini, F. Ruggiero, F. Zimmermann, M. Zorzano-Mier, Preprint CERN-SL-Note-2000-048-MD (2000)
- [14] W. Fischer, T. Satogata and R. Tomas, *Measurement of Transverse Echoes in RHIC*, Proceedings of PAC2005, 1955 (2005)
- [15] T. Sen and W. Fischer, *Diffusion Measurement from Observed Transverse Beam Echoes*, Phys. Rev. AB **20**, 011001 (2017)
- [16] G. Stancari, *Measurement of Beam Halo Diffusion and Population Density in the Tevatron and in the Large Hadron Collider*, Proceedings of HB2014, 294 (2014).
- [17] A.W. Chao, Lecture Notes at www.slac.stanford.edu/~achao/lecturenotes.html
- [18] R. E. Meller, A.W. Chao, J.M. Petersen, S.G. Peggs and M. Furman, SSC-N-360 (1987)
- [19] D. Edwards and M.J. Syphers, *An Introduction to the Physics of High Energy Accelerators*, Wiley

- [20] I.S. Gradshteyn and I.M. Ryzhik, *Table of Integrals, Series and Products*, Academic Press (1983)
- [21] M. Abramowitz and I. A. Stegun, *Handbook of Mathematical Functions*, Dover Publications
- [22] S. K. Lucas and H. K. Stone, *Evaluating infinite integrals involving Bessel function integrands of arbitrary order*, *J.Comp.App.Math.*, **64**, 217 (1995)
- [23] T. Sen, B. Erdelyi, M. Xiao and V. Boochoa, *Beam-beam effects at the Fermilab Tevatron: Theory*, *Phys. Rev. AB*, **7**, 041001 (2004)